

# Time-Domain Response of ECG Bioelectric Amplifiers

M. J. BURKE, O. TUOHY

Dept. of Electronic and Electrical Engineering,  
Trinity College, University of Dublin,  
College Green, Dublin 2,  
IRELAND

mburke@tcd.ie

<http://www.tcd.ie/eleceng/>

**Abstract:** This paper investigates the low-frequency response of a multi-stage bioelectric amplifier intended for use in the measurement of the electrocardiogram (ECG) using dry contact electrodes. These electrodes have an impedance which is typically an order of magnitude greater than that of the standard disposable self-adhesive electrodes used in clinical ECG recording. The design was undertaken with the intention of exploiting micro-power CMOS operational amplifier technology to minimise power in ambulatory recording. The response is optimised to meet the transient response requirements of the International Electrotechnical Commission Standard 60601 applying to electrocardiographs [1,2]. The optimum configuration was established to be two differential stages with a gain of 20dB each and a differential-to-single-ended output stage having unity gain. The -3dB pole is placed at 0.013Hz in the first and second stages to give an overall -3dB low cut-off frequency of 0.02Hz. In addition, a zero at 0.0013Hz in the non-inverting front-end stage was cancelled by the pole of the input ac coupling network. This ensured that the maximum undershoot of 100 $\mu$ V and the maximum recovery slope of 300 $\mu$ Vs<sup>-1</sup> permitted in response to a narrow pulse of 3mV amplitude and 100ms duration were met.

**Key-Words:** - ECG Recording, Bioelectric Amplifiers, Dry Electrodes, Un-gelled Electrodes.

## 1 Introduction

The low-frequency response of the bioelectric amplifiers used in the recording of the human electrocardiogram (ECG) is of the utmost importance due to the clinical significance of such recordings. Appropriate magnitude and phase responses are needed in order to prevent distortion of the ECG signal profile and degradation of the waveform morphology. The nature of the distortion which can arise in the ECG signal due to poor low frequency response in the recording amplifier has been well documented over the years and has serious diagnostic implications [3,4]. The distortion which results from poor low frequency response has a detrimental effect primarily on the T-wave, the S-T segment and the Q-T interval, but can also introduce anomalies into the higher frequency QRS complex [5,6]. In the past decade or so, there has been a substantial increase in the number of portable ECG recorders that are used in non-clinical scenarios such as general practice, sports medicine, physiology laboratories and even on the factory floor. This has led to an increase in battery-operated, portable equipment and the associated changes in instrumentation and circuitry, with trends towards much lower power consumption. Consequently, techniques have changed in the design of the electronic amplifiers for ECG recording. Lower

power supply voltages have tended to make amplifier front-end stages ac coupled rather than dc coupled as in the past. This allows electrode polarisation voltages to be eliminated at the input so that they do not saturate the front-end stage of the amplifier. Recent advances in electrode technology have increased the magnitude of these polarisation voltages. Ac coupling also facilitates incorporating a high gain into the front-end stage of the amplifier in order to preserve the signal-to-noise ratio. The introduction of micro-power CMOS technology has also meant that the gain-bandwidth product of operational amplifiers has fallen. As a result, the gain required in low-power ECG amplifiers is by necessity usually spread over several stages. This has led to an increase in multi-stage amplifier configurations and a consequent increase in the complexity of the associated frequency response at both the high and low ends of the spectrum. The authors investigate the low-frequency response of a multi-stage bioelectric amplifier intended for use in ECG signal recording using un-gelled or dry electrodes. In particular, the low-frequency configuration of the circuitry is optimised in order to guarantee that the transient response to a narrow pulse of 3mV amplitude and 0.1s duration is met.

## 2 Background

Standards for the performance requirements of ECG recorders have been developed in the US by the American National Standards Institute (ANSI) with recommendations made by the American Heart Association (AHA) and in Europe by the International Electrotechnical Commission (IEC). These have changed much over the decades since they were first introduced and have taken account of technological developments. Most recent standards have made an effort to merge the US and EU requirements to make them almost identical. This has, in fact, added strength to both sets of standards and increased the usage of the IEC 60601 standard, which is now accepted worldwide [1,2].

### 2.1 Frequency domain requirements

Early standards for ECG recorder performance were based on recommendations issued by the AHA and the IEEE in 1967 [7,8]. These standards required that the magnitude of the frequency response be within  $\pm 0.5\text{dB}$  of the mid-band gain within the frequency range  $0.67\text{Hz} - 150\text{Hz}$ . The low-frequency value is based on a practical minimum heart rate of 40 beats-per-minute (bpm). The phase shift was required to be no greater than that of a single-pole high-pass filter having a  $-3\text{dB}$  cut-off frequency of  $0.05\text{Hz}$  [7,8]. These magnitude and phase response requirements are shown in Fig.1.

More recent standards issued by both the EU and the US [1,2] require that the amplitude response of an ambulatory ECG recorder shall be within  $\pm 3\text{dB}$  of the response at  $5\text{Hz}$ , within a frequency band of  $0.05\text{Hz}$  to at least  $55\text{Hz}$ . A phase response requirement is not specified but the merits of a single-pole high-pass filter having a cut-off frequency of  $0.05\text{Hz}$  are still cited as a benchmark. Instead of the phase response requirement a time-domain specification has been introduced.

### 2.2 Time domain requirements

The IEC 60601 most recent standards, which are now closely aligned and merged with those of ANSI, have introduced two time-domain methods of testing ECG recorder performance. These are both shown in Fig.2. Method A was introduced in a previous IEC standard and stipulates the response to a narrow rectangular pulse of  $3\text{mV}$  amplitude and  $100\text{ms}$  duration with a repetition rate of 1 pulse per second. The maximum undershoot from the baseline allowed is  $100\mu\text{V}$  and the maximum recovery slope permitted following this undershoot is  $300\mu\text{Vs}^{-1}$ , as indicated in Fig.2. Method B, on the other hand, uses a triangular wave to model the QRS complex

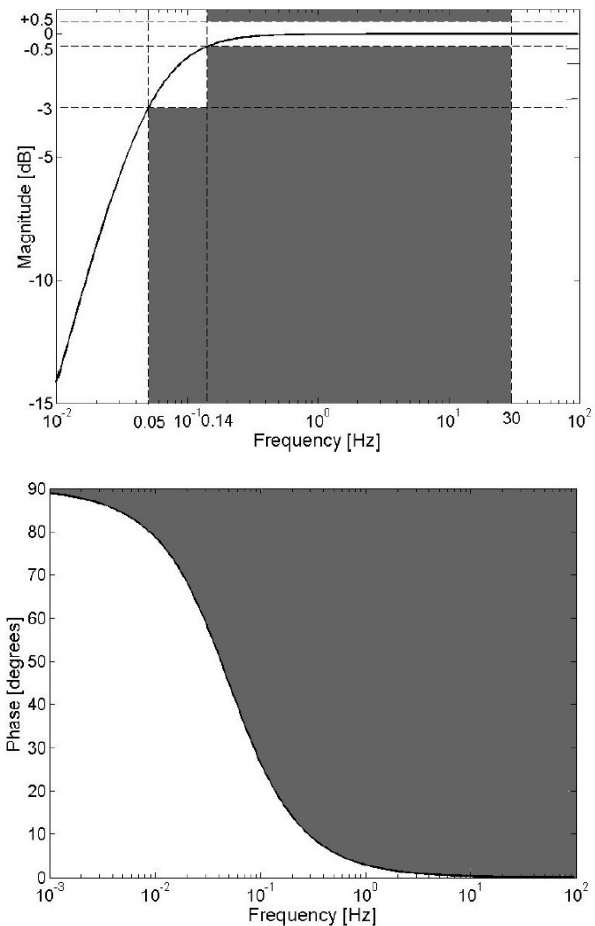


Fig.1 Magnitude and Phase Requirements.

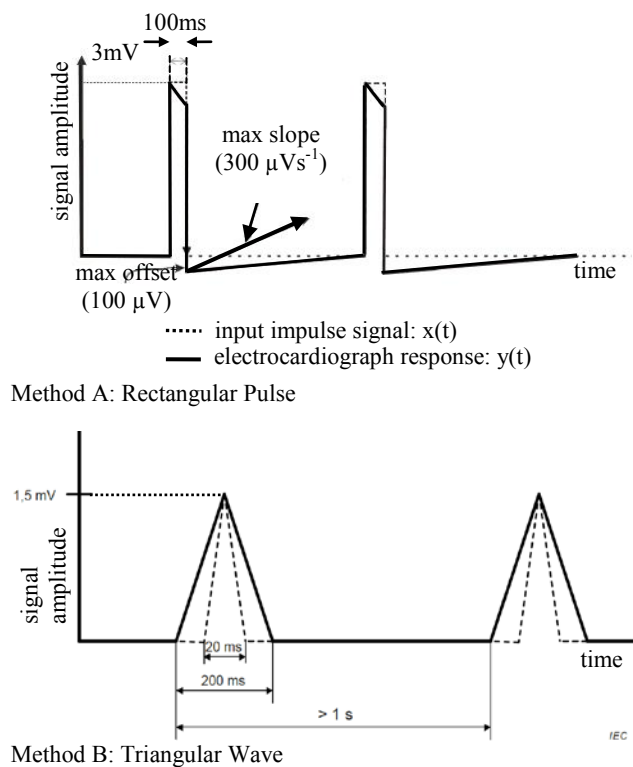


Fig.2 Transient Response Requirements [1,2].

of the ECG signal. An isosceles triangular wave having a peak amplitude of 1.5mV and a duration varying between 20ms and 200ms with a repetition rate of less than 1Hz is applied as input to the recorder. The amplitude of the peak of the triangle must maintain a variation within +0dB and -1dB (-12%) as the pulse duration is varied between 20ms and 200ms. This can be seen in Fig.2. In the studies carried out by the authors, the rectangular pulse of Method A was preferred for assessment of the transient response.

### 3 Single-Stage Amplifiers

#### 3.1 Unity Gain Single-Pole High-Pass Filter

In biomedical applications the dynamic signal of interest is often superimposed on a large dc or very slowly varying baseline and consequently ac coupling is required to extract the wanted signal from these. The first stage of interest is the single-pole high-pass filter which has become a benchmark circuit for performance comparison with other bio-amplifier stages. A simple 1<sup>st</sup>-order unity-gain high-pass response can be obtained by including the network consisting of resistor  $R_3$  and capacitor  $C_3$  at the input of a buffer amplifier as shown in Fig.3. This configuration was used as the reference standard in the early performance specifications [7,8] where the -3dB cut-off frequency was set at 0.05Hz. It is still cited as a comparative reference in more recent specifications [1,2]. If the bandwidth of the op-amp is considered as unlimited for convenience in this case, then the steady-state transfer function of this stage is given as:

$$\frac{V_o(\omega)}{V_i(\omega)} = \frac{j\omega C_3 R_3}{1 + j\omega C_3 R_3} = \frac{j\left(\frac{\omega}{\omega_{p1}}\right)}{1 + j\left(\frac{\omega}{\omega_{p1}}\right)} \quad (1)$$

where the radian pole frequency is  $\omega_{p1} = 1/C_3 R_3$ . There is also a zero located at  $\omega = 0$ . The steady-state magnitude and phase vs frequency responses of this filter are given as:

$$\left| \frac{V_o(\omega)}{V_i(\omega)} \right| = \frac{\omega C_3 R_3}{\sqrt{1 + \omega^2 C_3^2 R_3^2}} \quad (2)$$

and

$$\phi(\omega) = \tan^{-1} \frac{1}{\omega C_3 R_3} \quad (3)$$

Idealised Bode plots of the magnitude and phase of the frequency response are also shown in Fig.3. The high-frequency pass-band gain is unity. The pole at the radian frequency  $\omega_{p1} = 1/C_3 R_3$  corresponds to the -3dB cut-off frequency of the high-pass response.

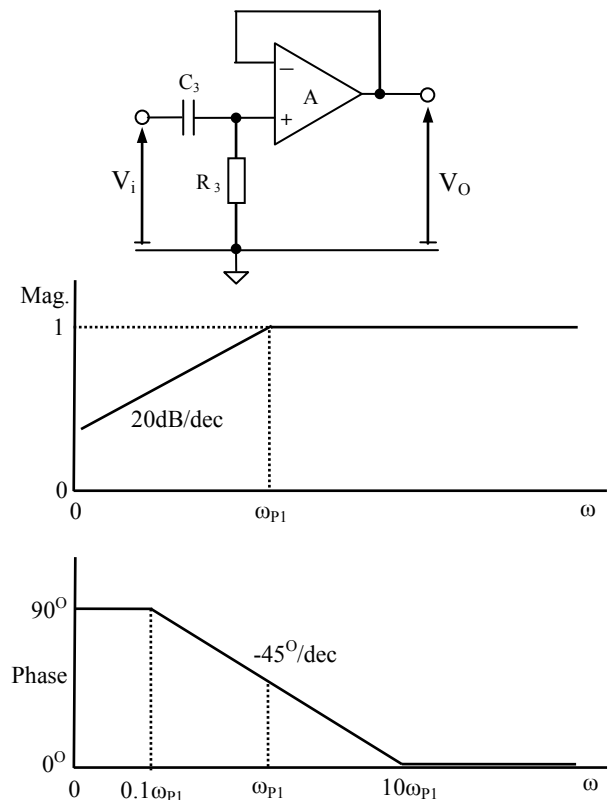


Fig.3 Magnitude & Phase Response of 0.05Hz HPF.

The transient response of this filter in the time domain can best be evaluated by treating the pulse as the sum of two step functions. A positive step of amplitude  $V_m$  which occurs at time  $t = 0$  is followed by a negative step of amplitude  $-V_m$  at a time  $t = T$  where  $T$  is the duration of the pulse. This means that the input voltage to the filter can be described as:

$$V_i(t) = V_m u(t) - V_m u(t - T) \quad (4)$$

This can be described in Laplace terms as:

$$V_i(s) = \frac{V_m}{s} - \frac{V_m}{s} e^{-sT} = \frac{V_m}{s} (1 - e^{-sT}) \quad (5)$$

The transfer function of the filter can be described in Laplace terms as:

$$\frac{V_o(s)}{V_i(s)} = \frac{s}{s + \frac{1}{C_3 R_3}} = \frac{s}{s + p} \quad (6)$$

where the pole is located at  $s = -p = -1/C_3 R_3$ . The output from the filter in response to the narrow pulse, expressed in Laplace terms is then:

$$V_o(s) = \frac{s}{s + p} V_i(s) = \frac{s}{s + p} \frac{V_m}{s} (1 - e^{-sT}) \quad (7)$$

Taking the inverse Laplace transform, the transient output voltage response is then given in the time domain as:

$$V_o(t) = V_m e^{-pt} u(t) - V_m e^{-p(t-T)} u(t - T) \quad (8)$$

Following the end of the pulse at  $t \geq T$  this becomes:

$$V_o(t) = -V_m(e^{pT} - 1)e^{-pt} \quad (9)$$

The magnitude of the voltage undershoot from the baseline at the end of the pulse at  $t = T$  is given as:

$$V_o(t=T) = V_m(1 - e^{-pT}) \quad (10)$$

For the pulse described in Fig.2,  $V_m = 3mV$  and  $T = 100ms$ . If the cut-off frequency of the filter is set at 0.05Hz, then  $p = 2\pi f_c = 0.314$  and the time constant required is  $C_3R_3 = 3.18s$ . This gives a value of undershoot of  $93\mu V$ , which is just inside the limit of the IEC 60601 performance standard.

The value of the recovery slope, following the end of the pulse can be found from the derivative of the output voltage described by Eq.9. In this case:

$$\frac{dV_o(t)}{dt} = pV_m(e^{pT} - 1)e^{-pt} \quad (11)$$

At the beginning of the recovery phase when  $t = T$ , the value of the slope is given as:

$$\left. \frac{dV_o(t)}{dt} \right|_{t=T} = pV_m(e^{pT} - 1)e^{-pT} \quad (12)$$

which becomes:

$$\left. \frac{dV_o(t)}{dt} \right|_{t=T} = pV_m(1 - e^{-pT}) \quad (13)$$

Again, for the pulse described in Fig.2,  $V_m = 3mV$ ,  $T = 100ms$  and for the high-pass filter  $p = 0.314$ . This gives a value of the recovery slope at the end of the pulse of  $29\mu V s^{-1}$ . This is well within the requirements of the IEC 60601 standard. The time-domain transient response of the single-pole high-pass filter of Fig.3 to the narrow pulse defined in Fig.2 is shown in Fig.4. These plots have been obtained from simulations of the circuit in MultiSim using the OPA379 op-amp (Texas Instruments Inc.) model and a range of cut-off frequencies. The bold curve in the plot represents the response of the filter with a cut-off frequency of 0.05Hz and verifies the values established above for the undershoot and recovery slope. These responses were obtained when the pulse was assumed to be generated using a

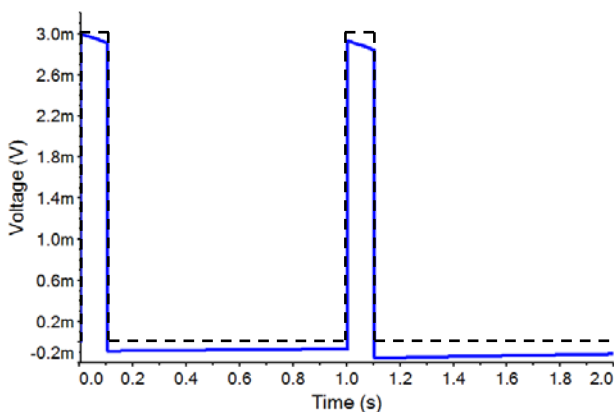


Fig.4 Narrow Pulse Response of 0.05Hz HPF.

voltage source which is connected directly to the filter.

### 3.2 Non-Inverting High-Pass Gain Stage

The next stage of interest is an amplifier stage that combines gain with a high-pass filter response. This is shown in the schematic diagram of Fig.5. In the first instance this stage is dc coupled to its input source in order to highlight an issue in the frequency response which is often overlooked.

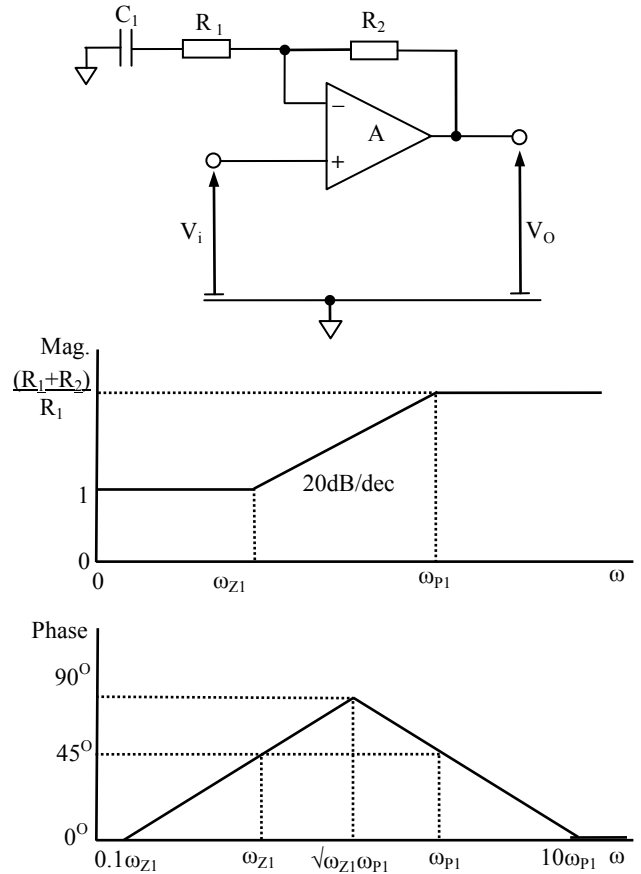


Fig.5. Magnitude & Phase of Non-Inverting Amp.

The transfer function of this stage is given as:

$$\frac{V_o}{V_i} = \frac{[1 + j\omega C_1(R_1 + R_2)]}{(1 + j\omega C_1 R_1)} = \frac{1 + j\left(\frac{\omega}{\omega_{z1}}\right)}{1 + j\left(\frac{\omega}{\omega_{p1}}\right)} \quad (14)$$

where  $\omega_{p1} = 1/C_1R_1$  and  $\omega_{z1} = 1/C_1(R_1+R_2)$

Bode plots of the magnitude and phase of the transfer function are included in Fig.5. It can be seen that the in-band high-frequency gain is given for  $\omega \rightarrow \infty$  as  $A_{V0} = (R_1 + R_2)/R_1$ . The pole location  $\omega_{p1}$  defines the -3dB cut-off frequency for the high-pass filter response. However, it should be noted that at the location of the zero,  $\omega_{z1}$ , the magnitude of the gain becomes unity and remains so down to dc.

This means that there is no rejection of low-frequency artefact or baseline drift. Conversely it does allow a dc bias voltage level to be maintained and passed on to a subsequent amplifier stage. It should also be noted that the ratio of the pole and zero frequencies is equal to the closed-loop mid-band gain of the amplifier, i.e.  $\omega_{p1}/\omega_{z1} = A_{V0}$ .

The phase can be seen to be zero at low frequencies, then to rise at a rate of  $45^\circ/\text{dec}$  from a frequency of  $0.1\omega_{z1}$  a decade below the location of the zero. It reaches its maximum value at a frequency of  $\sqrt{\omega_{z1}\omega_{p1}}$  which is the geometric mean of the pole and zero locations. The phase then decreases thereafter at a rate of  $-45^\circ/\text{dec}$  returning to zero at a frequency of  $10\omega_{p1}$  a decade above the location of the pole. If the pole and zero locations are separated by more than two decades the phase will reach a plateau at  $90^\circ$  between the frequencies a decade above the location of the zero,  $10\omega_{z1}$  and a decade below the location of the pole,  $0.1\omega_{p1}$ .

### 3.3 AC Coupled High-Pass Gain Stage

The final single-stage amplifier of interest is an amplifying stage which incorporates ac coupling of the input signal. This is accomplished by including the network consisting of the resistor  $R_3$  and the capacitor  $C_3$  to block dc voltages and suppress low-frequency artefact and baseline drift. The schematic diagram of this stage is shown in Fig.6. This stage has a steady-state transfer function of the form:

$$\frac{V_o}{V_i} = \frac{(j\omega C_3 R_3)[1 + j\omega C_1(R_1 + R_2)]}{(1 + j\omega C_3 R_3)(1 + j\omega C_1 R_1)} \quad (15)$$

It can be seen that this stage has an in-band high-frequency gain of  $A_V = (R_1 + R_2)/R_1$ . The -3dB pole in the high-pass response is again located at a radian frequency of  $\omega_{p1} = 1/C_1 R_1$ . As for the previous circuit, there is a zero in the response located at a frequency of  $\omega_{z1} = 1/C_1(R_1 + R_2)$ . There is also, however a second pole introduced by the input coupling network and located at a frequency given by  $\omega_{p2} = 1/C_3 R_3$ . The transfer function of this stage can therefore also be written as:

$$\frac{V_o}{V_i} = \frac{j\left(\frac{\omega}{\omega_{z2}}\right)\left[1 + j\left(\frac{\omega}{\omega_{z1}}\right)\right]}{\left[1 + j\left(\frac{\omega}{\omega_{p2}}\right)\right]\left[1 + j\left(\frac{\omega}{\omega_{p1}}\right)\right]} \quad (16)$$

Bode plots of the magnitude and phase of this stage are also shown in Fig.6. If the input ac coupling network  $C_3$ - $R_3$  were omitted, the gain of this stage would level out at unity, at the zero in the frequency response which is located at a radian frequency of  $\omega_{z1} = 1/C_1(R_1 + R_2) = \omega_{p1}/A_{V0}$  as shown by the

dashed line in the magnitude response of Fig.6. The zero would also have the effect of restoring the low-frequency phase back to zero as  $\omega \rightarrow 0$ , again shown by the dashed line in the phase response of Fig.6.

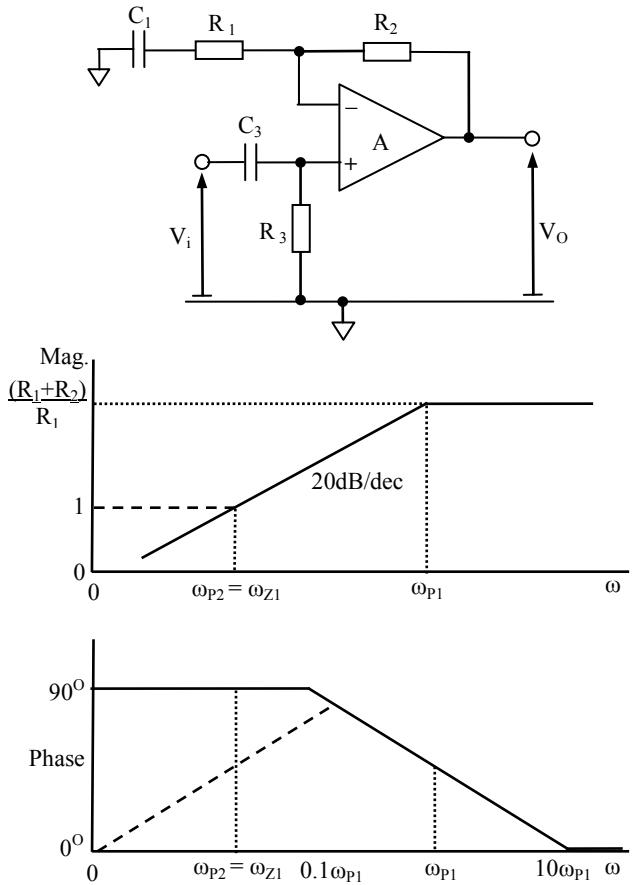


Fig.6. Magnitude & Phase of 1-Stage HP Amplifier

The effect of the second pole introduced by the coupling network is to ensure that the magnitude attenuation continues down through low frequencies to dc which blocks these components. It also means that the low-frequency phase shift levels out at  $90^\circ$  at low frequencies and does not return to zero. This can be seen from the solid line plots of Fig.6. In order to get an overall response in the form of a high-pass filter, the lower frequency pole,  $\omega_{p2}$ , of the input network is arranged to cancel the zero in the response of the feedback network by a choice of time constants such that  $C_3 R_3 = C_1(R_1 + R_2)$ . In this case the transfer function of the stage becomes:

$$\frac{V_o}{V_i} = \frac{j\omega C_3 R_3}{(1 + j\omega C_1 R_1)} = \frac{j\omega C_1 (R_1 + R_2)}{(1 + j\omega C_1 R_1)} \quad (17)$$

The magnitude and phase responses in this case are depicted by the solid lines in the plots of Fig.6.

Fig.7 shows the transient response of this amplifier stage to the narrow 100ms pulse defined in Fig.2. The plots are input referred to allow for the

gain of 20dB of this stage when applying the performance criteria. The lighter curves show the effect of some mismatch between the pole at  $\omega_{P2}$  and the zero at  $\omega_{Z1}$ . The bold curve shows the response for perfect pole zero cancellation,  $\omega_{P2} = \omega_{Z1}$  and a -3dB cut-off frequency of  $f_{C1} = 0.05\text{Hz}$ . In the latter case the voltage undershoot and recovery slope values are the same as for the simple single-pole filter of Fig.3.

It should be pointed out, however, that the large time-constant of the input coupling network  $C_3R_3 = C_1(R_1 + R_2)$  required to accomplish the pole-zero cancellation can lead to long initialisation times on power-up of the amplifier or during recovery from overload conditions.

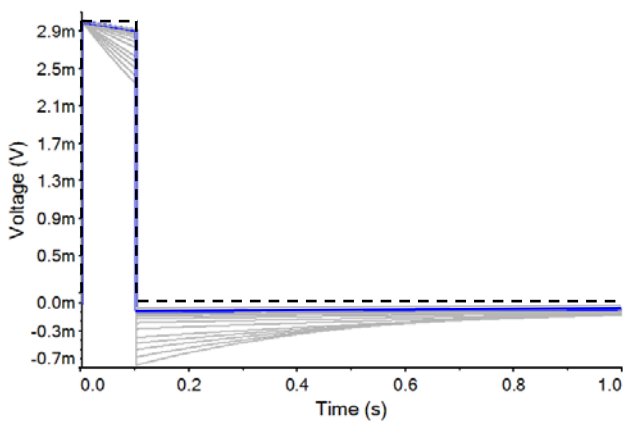


Fig.7 Transient Response of 1-Stage HP Amplifier

## 4 Multi-Stage Amplifiers

### 4.1 Two-Stage Differential Amplifier

The schematic diagram of a simple differential amplifier is shown in Fig.8. This has a single cross-coupled input stage with differential input voltages  $V_1$  and  $V_2$ . This is followed by the standard

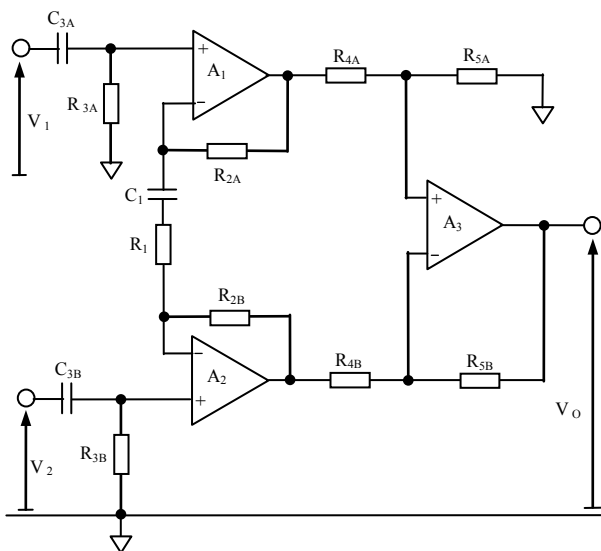


Fig.8 Schematic Diagram of Differential Amplifier

differential-to-single-ended conversion stage which provides the output voltage,  $V_O$ . The A and B designations of components will nominally have the same values. The steady-state transfer function of this amplifier structure is given for a differential input  $V_1 - V_2$  as:

$$\frac{V_o}{V_1 - V_2} = \frac{R_5 [1 + j\omega C_1 (R_1 + 2R_2)] (j\omega C_3 R_3)}{R_4 (1 + j\omega C_1 R_1) (1 + j\omega C_3 R_3)} \quad (18)$$

Very often  $R_5 = R_4$  so that the output stage has unity gain, in order to maximize the CMRR. In this case the in-band differential gain of this stage is given as  $A_{V0} = (R_1 + 2R_2)/R_1$ . The -3dB cut-off frequency is again located at  $\omega_{P1} = 1/C_1R_1$  while the zero is located at  $\omega_{Z1} = 1/C_1(R_1 + 2R_2) = \omega_{P1}/A_{V0}$ . The pole due to the input ac coupling network, which is identical at each input terminal, is again located at a frequency  $\omega_{P2} = 1/(C_3R_3)$ . The same pole-zero cancellation mechanism as used in the single-stage amplifier can be implemented in the differential amplifier by choosing  $C_3R_3 = C_1(R_1 + 2R_2)$ . The transient response in the time domain to the pulse of Fig.2 is shown in Fig.9. These plots are again input referred to allow for the gain of the stage and show the detail at the lower end of the trailing edge of the pulse. The value of undershoot of  $97\mu\text{V}$  and the recovery slope of  $30\mu\text{Vs}^{-1}$  again meet the IEC 60601 performance as in the case of the simpler gain stages.

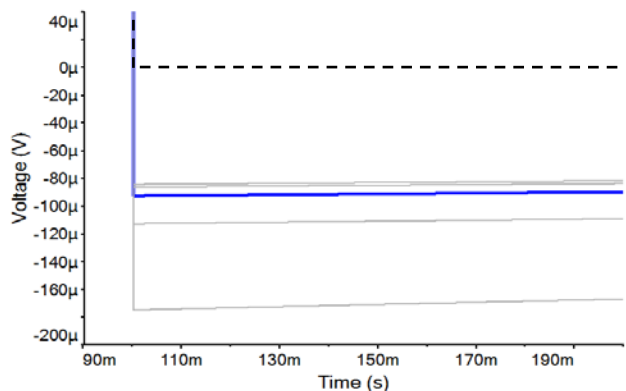


Fig.9 Trailing Edge Response of 2-Stage Amplifier

### 4.2 Three-Stage Differential Amplifier

The final configuration of interest is the 3-stage amplifier shown in Fig.10 where component values are omitted since many change in testing [9]. This has a high-pass input differential stage and a differential-to-single-ended output stage, identical to the 2-stage amplifier. There is a second differential stage that is dc coupled to the first so that the output dc bias conditions of the first stage carry through to the second stage. The ac coupling of the first stage is sufficient to block dc polarisation potentials of

electrodes appearing at the amplifier input. The transfer function of the 3-stage amplifier is given as:

$$\frac{V_o}{V_1 - V_2} = \frac{R_5}{R_4} \times \frac{[1 + j\omega C_1(R_1 + 2R_2)][1 + j\omega C_7(R_7 + 2R_6)](j\omega C_3 R_3)}{(1 + j\omega C_1 R_1)(1 + j\omega C_7 R_7)(1 + j\omega C_3 R_3)} \quad (19)$$

where,  $R_6$ ,  $R_7$  and  $C_7$  are the components in the second differential stage. It can be seen that the dc coupling in the second differential stage adds an additional pole and zero to the transfer function. If the output stage has unity gain and the overall gain is shared equally between the two differential stages then the poles and zeros of both of these stages are identical so that  $\omega_{p1} = 1/(C_1 R_1) = \omega_{p3} = 1/(C_7 R_7)$  and  $\omega_{z1} = 1/[C_1(R_1 + 2R_2)] = \omega_{p1}/A_{V1} = \omega_{z2} = 1/[C_7(R_7 + 2R_6)] = \omega_{p3}/A_{V2}$ . The gains of the individual differential stages were maintained at 20dB, as for the two-stage amplifier, so that the overall gain of the three-stage amplifier is 40dB. The pole-zero cancellation is maintained in the first differential stage as in the 2-stage amplifier by the choice  $C_3 R_3 = C_1(R_1 + 2R_2)$ . If the intention, in the first instance, is to maintain the -3dB frequency of the three-stage amplifier at the same location as for the two-stage amplifier then it can be shown that:

$$\omega_{-3dB2} = \sqrt{\sqrt{2} - 1} \omega_{-3dB} = 0.645 \omega_{-3dB1} \quad (20)$$

where  $\omega_{-3dB2}$  is the -3dB frequency of an individual differential stage in a two-stage cascade having identical stages and  $\omega_{-3dB1}$  is the -3dB frequency of a single-stage differential amplifier in isolation. The overall -3dB frequency of the two cascaded differential stages should be equal to the -3dB high-pass cut-off frequency required in the amplifier as a whole. From eq.20, it can be established that with  $f_{-3dB} = 0.05\text{Hz}$  then  $f_{-3dB2} = 0.032\text{Hz}$  to maintain an overall -3dB frequency of 0.05Hz in the three-stage amplifier. However, while this choice satisfies the frequency-domain performance requirements, it does not meet the transient response requirements to the narrow pulse of Fig.2. In order to accomplish the latter, it is necessary to lower the overall -3dB frequency of the three-stage amplifier to 0.043Hz which corresponds to a -3dB frequency for the individual differential stages of 0.028Hz. When this is done, the undershoot in the pulse response is maintained at  $98\mu\text{V}$  and the recovery slope at  $15\mu\text{Vs}^{-1}$ . This can be seen from the time-domain response of Fig.11, expanded in the region at the trailing edge of the pulse. The lower heavy curve indicates the response of the 3-stage ECG amplifier while the upper heavy curve indicates the response of a single-stage amplifier with a -3dB cut-off frequency of 0.05Hz for comparison. These responses fall within the limits in the IEC 60601 performance standard for ECG recorders.

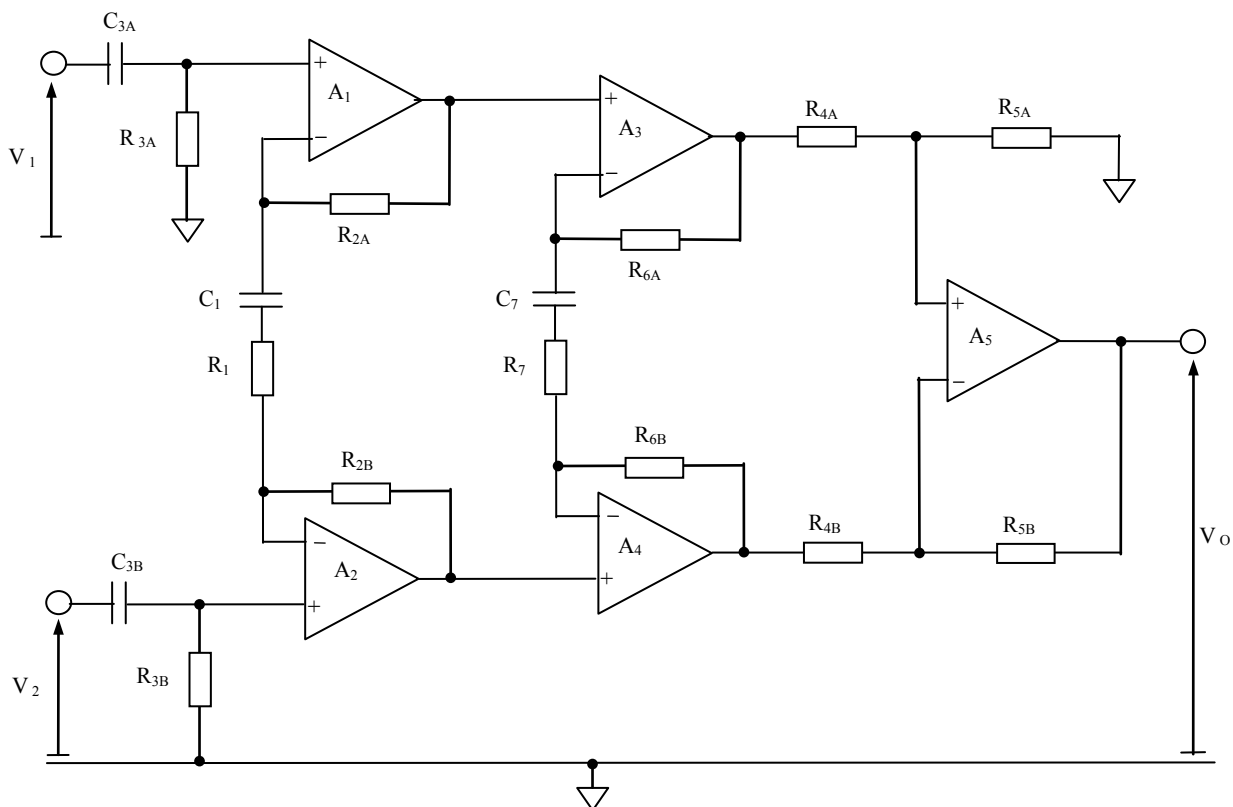


Fig.10. Schematic Diagram of a 3-Stage ECG Amplifier.

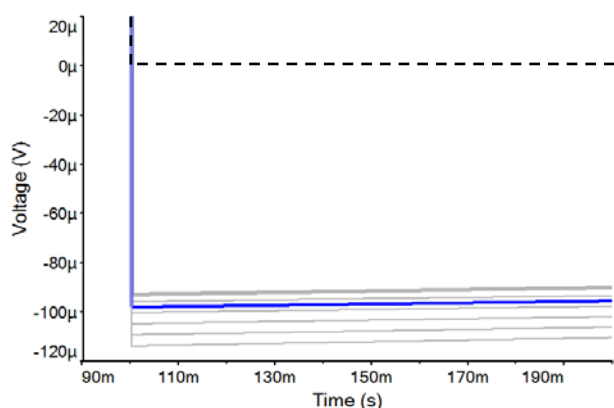


Fig.11. Pulse Response of 3-Stage ECG Amplifier

### 5 Effect of Electrode Impedance

All of the amplifier circuit configurations examined in the previous sections assume that the input signal provided to the amplifier is generated by an ideal voltage having zero internal impedance. The purpose of the ECG recording amplifier is to provide a signal which accurately represents the electrical potential existing on the surface of the patient’s body. Therefore the amplifier cannot be considered in isolation. The IEC 60601 specification does not take this into consideration in the measurement of the steady-state frequency response and the transient time-domain response. No equivalent electrical model is suggested for the electrodes which are used to detect the ECG signal. However, in the case of other measurements such as CMRR, an electrical model of source impedance is stipulated. The IEC 60601 specification also recommends a minimum input impedance for clinical ECG amplifiers of 10MΩ.

#### 5.1 Electrode Electrical Model

The impedance of the electrodes used to provide the necessary interface between the patient’s skin and the amplifier must be treated as an intrinsic part of the recording system. The IEC 60601 standard specifies a simple electrode model of a single parallel C-R network with  $C = 47\text{nF}$  and  $R = 51\text{k}\Omega$  for CMRR measurements. This is inserted in series with each amplifier input when injecting signals from a test signal generator. This simplified model does not provide an accurate reflection of all of the effects that are present when using surface electrodes. In particular, it does not accurately model the un-gelled electrodes that are becoming more popular in modern portable recording equipment. Previous work has shown that surface bio-electrodes are modelled more accurately by the network shown in Fig.12. This model consists of two parallel C-R networks with two series resistors.

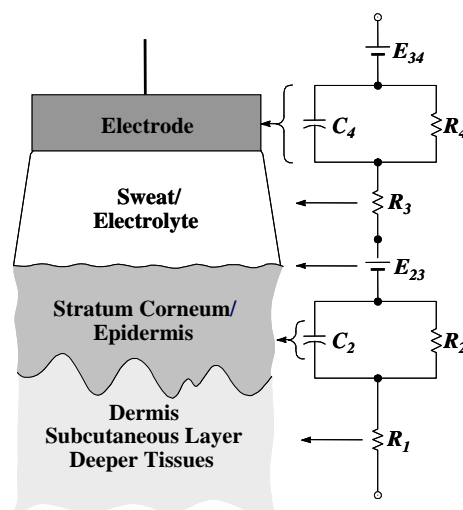


Fig.12. Electrical Model of Bioelectrode

The dc voltages represent polarisation potentials that will be blocked from the input of the amplifier by the use of ac coupling. Previous studies of electrodes have yielded the values of the model components for a number of un-gelled or dry ECG recording electrodes [10,11]. For this study component values were selected that represent the extremes of the associated time constants involved. Electrode models used include: the single C-R network specified in the IEC 60601 standard, a double C-R model with component values obtained from stainless-steel contact electrodes, and two double C-R models representative of conducting rubber electrodes. The values of the components for these models are listed in Table 1.

Table 1: Properties of Electrode Models

Electrode Model	Single C-R (IEC)	Stainless Steel 2 - CR	Conductive Rubber #1 2 - CR	Conductive Rubber #2 2 - CR
$R_1+R_3$ (kΩ)	NA	5	12	5
$C_2$ (µF)	0.047	878	220	432
$R_2$ (kΩ)	51	256	267	72
$\tau_2$ (s)	0.002	225	59	31
$C_4$ (µF)	NA	56	23	6.9
$R_4$ (kΩ)	NA	380	380	158
$\tau_4$ (s)	NA	21	8.6	1.1

#### 5.2 Time Response of Electrode & Amplifier

Tests were carried out to investigate the effects of varying both the impedance of the recording electrodes and the input impedance of the amplifier on the transient response in the time domain to the narrow pulse of Fig. 2. Each of the electrode models listed in Table 1 was used in combination with four values of common-mode input impedance of the amplifier,  $R_3$ , namely: 1MΩ, 10MΩ, 100MΩ and 1GΩ. This was done firstly for the 2-stage amplifier

of Fig.8. The value of the time-constant  $C_1R_1$  was kept fixed as required to provide a -3dB low cut-off frequency of 0.05Hz for the cascaded stages. The low-frequency pole-zero cancellation was maintained by changing the value of the input blocking capacitor  $C_3$  when the value of the input resistance  $R_3$  was altered in order to keep the time constant  $C_3R_3 = C_1(R_1 + 2R_2)$ .

Table2: Pulse Response, 2-Stage Amp,  $f_{-3dB}=0.05\text{Hz}$

Electrode Model ↓	Amplifier $R_3$ ( $M\Omega$ ) →	1	10	100	1000
(IEC) Single C-R	Undershoot ( $\mu\text{V}$ )	<b>157</b>	<b>164</b>	<b>165</b>	<b>165</b>
	Recovery Slope ( $\mu\text{Vs}^{-1}$ )	174	188	200	200
Stainless Steel 2 - CR	Undershoot ( $\mu\text{V}$ )	<b>187</b>	<b>166</b>	<b>164</b>	<b>170</b>
	Recovery Slope ( $\mu\text{Vs}^{-1}$ )	233	205	203	203
Conductive Rubber #1 2 - CR	Undershoot ( $\mu\text{V}$ )	<b>554</b>	<b>206</b>	<b>168</b>	<b>164</b>
	Recovery Slope ( $\mu\text{Vs}^{-1}$ )	<b>3400</b>	<b>498</b>	213	185
Conductive Rubber #2 2 - CR	Undershoot ( $\mu\text{V}$ )	<b>486</b>	<b>199</b>	<b>173</b>	<b>165</b>
	Recovery Slope ( $\mu\text{Vs}^{-1}$ )	<b>2000</b>	<b>449</b>	235	185

The values of the undershoot and recovery slope in response to the pulse of Fig.2 are given in Table 2 for the range of input resistance examined. All values are referred back to the amplifier input for direct comparison with the input pulse. Values in bold type indicate a violation of the requirements of the IEC 60601 performance specification. It can be seen from the table that the undershoot requirement of less than  $100\mu\text{V}$  is violated by all electrode models for all values of amplifier input impedance. The recovery slope requirement of  $300\mu\text{Vs}^{-1}$  is satisfied by all electrode models for an input impedance of  $100M\Omega$  or greater but is violated by the conductive rubber electrodes for values of impedance below this.

The plots in Fig.13 show the time-domain response to the narrow pulse of the 2-stage amplifier with the cut-off frequency set at  $f_c = 0.05\text{Hz}$  when using the IEC single-CR electrode model, for the range of values of the input resistor  $R_3$  used. The vertical axis shows the amplitude on a scale of  $100\mu\text{V}/\text{div.}$  and the horizontal axis shows time on a scale of  $1\text{s}/\text{div.}$  The legend on the right of the diagram gives the value of the resistance  $R_3$  in  $M\Omega$ . It can be seen from these plots that for a given low cut-off frequency, in this case  $0.05\text{Hz}$ , the change in the input resistance has only limited effect. All of these plots indicate that the undershoot criterion is not satisfied for any value of resistor  $R_3$ .

The same set of tests was carried out on the 3-stage amplifier of Fig.10, with the overall -3dB low cut-off frequency  $f_{-3dB1} = 0.05\text{Hz}$  by choosing  $f_{-3dB2} =$

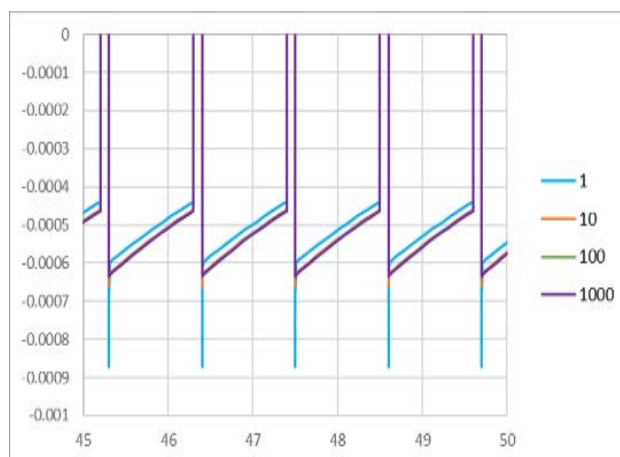


Fig.13 Pulse Response, 2-Stage Amp.,  $f_c = 0.05\text{Hz}$ .

0.03Hz for each of the differential stages considered individually. The results of these tests are shown in Table 3. A similar pattern of violations of the performance specification exist as for the 2-stage amplifier. All electrode models lead to a violation of the undershoot requirement for all values of amplifier input impedance. The recovery slope requirement is violated by the conductive rubber electrodes for an amplifier input impedance below  $100M\Omega$ , and by the single C-R model for less than  $1G\Omega$ .

Table3: Pulse Response, 3-Stage Amp,  $f_{-3dB}=0.05\text{Hz}$

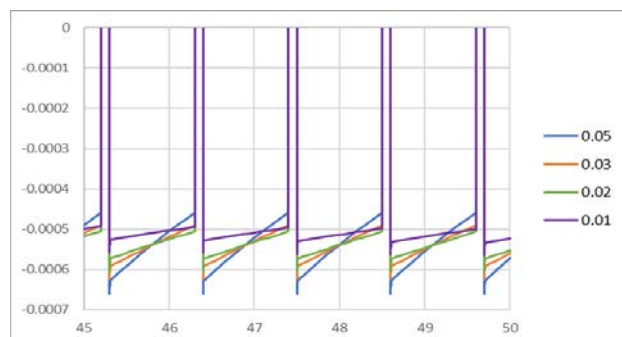
Electrode Model ↓	Amplifier $R_3$ ( $M\Omega$ ) →	1	10	100	1000
(IEC) Single C-R	Undershoot ( $\mu\text{V}$ )	<b>220</b>	<b>211</b>	<b>210</b>	<b>210</b>
	Recovery Slope ( $\mu\text{Vs}^{-1}$ )	<b>24000</b>	<b>2900</b>	<b>481</b>	252
Stainless Steel	Undershoot ( $\mu\text{V}$ )	<b>237</b>	<b>215</b>	<b>213</b>	<b>213</b>
	Recovery Slope ( $\mu\text{Vs}^{-1}$ )	281	251	248	248
Conductive Rubber #1 2 - CR	Undershoot ( $\mu\text{V}$ )	<b>647</b>	<b>258</b>	<b>216</b>	<b>212</b>
	Recovery Slope ( $\mu\text{Vs}^{-1}$ )	<b>3800</b>	<b>580</b>	281	251
Conductive Rubber #2 2 - CR	Undershoot ( $\mu\text{V}$ )	<b>553</b>	<b>249</b>	<b>217</b>	<b>213</b>
	Recovery Slope ( $\mu\text{Vs}^{-1}$ )	<b>3100</b>	<b>553</b>	276	252

Several further series of tests were subsequently carried out on the 3-stage amplifier while progressively decreasing the -3dB low cut-off frequency. Table 4 shows the results of the tests for  $f_{-3dB1} = 0.02\text{Hz}$  with  $f_{-3dB2} = 0.013\text{Hz}$ . It can be seen in this case that all of the electrode models meet both performance limits for an amplifier input impedance of  $100M\Omega$  or greater. This was identified as the highest value of the -3dB low cut-off frequency for which all electrode models met both performance requirements and was only possible with an input impedance of  $100M\Omega$ . The plots given

Table4: Pulse Response, 3-Stage Amp,  $f_{-3dB}=0.02\text{Hz}$ 

Electrode Model ↓	Amplifier $R_3$ ( $M\Omega$ ) →	1	10	100	1000
(IEC) Single C-R	Undershoot ( $\mu\text{V}$ )	<b>256</b>	<b>106</b>	90	88
	Recovery Slope ( $\mu\text{Vs}^{-1}$ )	<b>652</b>	147	100	94
Stainless Steel	Undershoot ( $\mu\text{V}$ )	<b>106</b>	84	81	80
	Recovery Slope ( $\mu\text{Vs}^{-1}$ )	122	94	90	90
Conductive Rubber #1 2 - CR	Undershoot ( $\mu\text{V}$ )	<b>537</b>	<b>129</b>	85	81
	Recovery Slope ( $\mu\text{Vs}^{-1}$ )	<b>3400</b>	<b>390</b>	118	91
Conductive Rubber #2 2 - CR	Undershoot ( $\mu\text{V}$ )	<b>399</b>	<b>122</b>	82	79
	Recovery Slope ( $\mu\text{Vs}^{-1}$ )	<b>2500</b>	<b>321</b>	109	88

in Fig.14 show the narrow pulse response of the 3-stage amplifier having a fixed input resistance of  $100M\Omega$ , for a range of values of  $-3\text{dB}$  low cut-off frequency. It can be seen that changing the cut-off frequency has a much more pronounced effect on the undershoot and recovery slope than the input resistance although both exert an effect.

Fig.14 Pulse Response, 3-Stage Amp,  $R_3 = 100M\Omega$ .

## 6 Conclusion

The existing IEC 60601 performance specification for ECG amplifiers suggests that a  $-3\text{dB}$  low cut-off frequency of  $0.05\text{Hz}$  and an input impedance of  $10M\Omega$  will meet the criteria of a maximum undershoot of  $100\mu\text{V}$  and a recovery slope of  $300\mu\text{Vs}^{-1}$  in the transient response to the narrow  $3\text{mV} - 100\text{ms}$  pulse of Fig.2. The authors have shown experimentally for a number of un-gelled electrode models that a 3-stage bioelectric amplifier needs to have a  $-3\text{dB}$  low cut-off frequency of  $\leq 0.03\text{Hz}$  and an input impedance of  $\geq 100M\Omega$  in order to meet these criteria. The electrode models used are typical of the un-gelled or lightly gelled electrodes that are becoming increasingly popular in clinical and ambulatory ECG measurements. Further work will be carried out to establish the amplifier requirements more analytically for these electrodes. However, the results of the experimental work presented in this paper suggest that a revision of the

impedance recommendations given in the IEC 60601 performance standard needs to be considered.

## References:

- [1] International Electrotechnical Commission, *Medical Electrical Equipment Std. 2-25*. IEC 60601, 2011.
- [2] International Electrotechnical Commission, *Medical Electrical Equipment Std. 2-47*. IEC 60601, 2012.
- [3] A. S. Berson and H. V. Pipberger, The Low-Frequency Response of Electrocardiographs: A Frequent Source of Recording Errors, *American Heart Journal*, Vol.71, 1966, pp. 779-789.
- [4] D. Tayler and R. Vincent, Signal Distortion in the Electrocardiogram Due to Inadequate Phase Response, *IEEE Transactions in Biomedical Engineering*, Vol.30, 1983, pp. 352-356.
- [5] M. J. Burke and M. Nasor, The Time Relationships of the Constituent Components of the Human Electrocardiogram, *Journal of Medical Engineering & Technology*, Vol.26, 1999, pp. 1-6.
- [6] M. J. Burke and G. Shorten, A Time Domain Based Classifier for ECG Pattern Recognition, *Proceedings of the 33rd IEEE Annual International Conference on Engineering in Medicine & Biology*, EMBC, Boston, 2011, pp. 4980-4983.
- [7] C. E. Kossmann et al., Recommendations for Standardization of Leads and of Specifications for Instruments in Electrocardiography and Vectorcardiography, *Circulation*, Vol.35, 1967, pp. 583-602.
- [8] H. V. Pipberger et al., Recommendations for Standardization of Instruments in Electrocardiography and Vectorcardiography, *IEEE Transactions in Biomedical Engineering*, Vol.14, 1967, pp. 60-68.
- [9] M. J. Burke and D. T. Gleeson, An Ultra-Low Power Pre-Amplifier for Painless Electrocardiography, *Proceedings of the 6<sup>th</sup> IEEE International Conference on Electronics, Circuits & Systems*, ICECS, Cyprus, 1999, pp. 615-619.
- [10] Baba, A. and Burke, M. J., Measurement of the Electrical Properties of Un-Gelled ECG Electrodes, *NAUN International Journal of Biological & Biomedical Engineering*, Vol.2, 2008, pp. 89-97.
- [11] M. J. Burke and M. V. Whelan, 'Photoplethymography: Selecting Opto-Electronic Components, *Medical & Biological Engineering & Computing*, Vol.24, 1986, pp. 647-650.